International Journal of Concrete Structures and Materials
DOI 10.1186/s40069-018-0254-7
ISSN 1976-0485 / eISSN 2234-1315

Ultrasonic Detection of Chloride Ions and Chloride Binding in Portland Cement Pastes

Arturo Emanuel Ramírez-Ortíz, Francisco Castellanos*, and Prisciliano F. de J. Cano-Barrita

(Received September 1, 2017, Accepted February 6, 2018)

Abstract: Chloride ions diffuse through the concrete cover and interact with the cement hydration products. As a result, some chloride ions become chemically and/or physically bound. Free chloride ions are the primary cause of steel corrosion in reinforced concrete structures. In this study, ultrasound was used to detect the presence and binding of chloride ions in cement pastes that contained supplementary cementing materials. Four cement pastes with w/c ratio of 0.55 were prepared and cast into cylindrical specimens that were moist cured for 254 days before being oven dried at 105 °C. The dried specimens were vacuum-saturated with NaCl solutions at various concentrations. Through-transmission ultrasonic measurements were performed as a function of time using 500 kHz longitudinal wave transducers. The results indicated exponential relationships between energy/amplitude weighted average frequency and the amount of chloride chemically bound by the cement pastes.

Keywords: ultrasound, X-ray diffraction, cement paste, chloride binding, durability.

1. Introduction

One of the primary factors that influences the durability of concrete structures is penetration of aggressive species such as chloride ions. Chloride ions present in concrete mix constituents, deicing salts, or marine environments are the main cause of steel corrosion in reinforced concrete structures (Neville 1995). Some of the chloride ions that penetrate the concrete cover become physically and chemically bound to the hydration products (Hirao et al. 2005; Marinescu and Brouwers 2012; Paul et al. 2015; Suryavanshi et al. 1996; Talero 2012; Thomas et al. 2012), while others remain free. Chemically bound chlorides form Friedel's salt. Free chlorides are present in the pore solution and cause corrosion of reinforcing steel upon reaching it at a certain threshold concentration (Ann and Song 2007; Glass and Buenfeld 1997; Grantham 2003; Saremi et al. 2002).

Conventional methods of determining the chloride ion resistance of concrete include the rapid chloride permeability test (ASTM C1202 2012), chloride ion migration tests (NT BUILD-492 1999), and profile grinding to determine the chloride ion concentration (NT BUILD-443 1995). Chloride binding isotherms reflect the chloride binding capacity of a specific cementitious material in concrete (Luping and Nilsson 1993). Most conventional techniques are destructive, time consuming, and expensive.

Non-destructive techniques have also been used to study chloride ion ingress in concrete. Torres-Luque et al. (2014) classified the non-destructive methods into three main groups: (i) ion selective electrodes (ISE) (Angst and Vennesland 2009; Atkins et al. 1996; Jin et al. 2017), (ii) electrical resistivity (ER) (Gao et al. 2017; Andrade et al. 2014; Hornbostel et al. 2013; Polder and Peelen 2002), and (iii) optical fiber sensors (OFS) (Falciai et al. 2001; Lam et al. 2009). Each technique has advantages and disadvantages. For instance, the ISE and OFS methods detect only free chloride ions. In addition, they must be installed before casting the concrete structure and thus cannot be used to monitor existing structures. While ER is easily performed on either new or existing structures, variations in ER measurements are influenced by various factors such as the degree of hydration, pore connectivity, moisture content, and pore solution composition. Magnetic resonance imaging (Cano et al. 2002) is a technique suitable for laboratory profiling of sodium and chloride distribution in cement-based materials. However, the low NMR sensitivity of ^{35}Cl makes its detection difficult, thus requiring the use of MRI systems with high-field superconducting magnets to increase signal intensity. These types of MRI systems are costly and not widely available, which restricts the use of MRI in studying cement-based materials. Recent studies have focused on the application of ground penetrating radar as a non-destructive method of studying the presence and penetration of chloride ions in cement-based materials (Dérobert et al. 2017; Hugenschmidt and Loser 2007; Kalogeropoulos et al. 2013; Senin and Hamid 2016). Researchers have also considered use of the near- and far-field microwave methods (Al-Mattarneh 2016; Chiniforush et al. 2017).

Instituto Politécnico Nacional/CIIDIR Oaxaca, Calle Hornos No. 1003, C. P. 71230 Santa Cruz Xoxocotlán, Oaxaca, Mexico.
*Corresponding Author; E-mail: fcastellanos@ipn.mx

Published online: 21 February 2018

Ultrasound (US) is a nondestructive monitoring technique used to assess the strength and deterioration of concrete. It has been used primarily to characterize concrete strength development (ACI Committee 228 2003), cracking (Aggelis et al. 2009), internal defects such as cracks, honeycombs and inclusions (Jung et al. 2002), porosity and permeability (Lafhaj et al. 2006), setting of high performance concrete (Lee et al. 2004; Trtnik et al. 2013) and deterioration of concrete by alkali-silica reactions (Gong et al. 2014; Ju et al. 2017). Several factors such as moisture content (Ohdaira and Masuzawa 2000), matrix density and porosity (Punurai et al. 2007), and pore fluid viscosity (Povey 1997) influence US measurements of cement-based materials. Increasing the NaCl concentration increases the solution density and viscosity (Lin and Brown 1993), which in turn increases the ultrasonic pulse velocity (UPV) and decreases the signal energy, respectively (Herzfeld and Litovitz 2013).

This paper proposes the basis for an experimental monitoring technique based on US that identifies the presence and binding of chloride ions in four hydrated cement pastes. These pastes exhibited differing chloride binding mechanisms and capacities, as determined via conventional chloride binding isotherms and by the height of the X-ray diffraction (XRD) peak that corresponded to Friedel's salt. After moist curing for 254 days, the samples were oven-dried at 105 °C and then vacuum saturated with NaCl solutions at concentrations of 0, 2.8, and 5.6 mol/L. US response signals from cement pastes were acquired from the vacuum saturated samples as functions of time for up to 200 days. The UPVs, energies, and average frequencies of the US signals were related to the presence and binding of chloride ions.

2. Experimental Investigation

2.1 Materials

Ordinary Portland cement (OPC), type F fly ash (FA), and silica fume (SF) were used with distilled water to prepare cement pastes. Table 1 provides the chemical compositions of the Portland cement and supplementary cementing materials used.

2.2 Method

2.2.1 Preparation and Conditioning of the Cement Paste Specimens

Four cement pastes with water-to-cement ratio (w/c) of 0.55 were prepared using 100% OPC, 90% OPC + 10% SF, 80% OPC + 20% FA, and 60% OPC + 40% FA. They were labeled as OPC, 10SF, 20FA, and 40FA, respectively. The cement pastes were prepared according to the ASTM C305 standard (ASTM C305 2011) and the proportions associated with cement replacement were determined by weight. Replacement of OPC with supplementary cementing materials produced cementitious systems with different chloride binding mechanisms. Physical binding of C–S–H dominated in the hydrated 10SF cement paste due to its high specific surface area (Byfors et al. 1986). Chemical chloride binding was more significant than physical adsorption in the 20FA and 40FA cement pastes (Talero 2012).

A total of 64 cylindrical cement paste specimens measuring 65 mm in diameter and 100 mm in length were cast using plastic molds. The molds were filled in two layers, each of which was compacted by tapping its base to expel trapped air. The specimens were then placed in a device designed to rotate at 7 rpm in order to minimize sedimentation in the fresh cement pastes. After 1 day, the specimens were demoulded and moist cured at 23 ± 2 °C via immersion in a saturated lime solution for 254 days. This long moist curing process was performed to obtain a high degree of hydration such that the effects of cement hydration during ultrasonic measurements would be negligible.

At 254 days, the specimens stored in saturated lime solutions were cut to 100 mm in length and further vacuum saturated (− 20 in-Hg) with deionized water for at least 1 h. After their masses were measured, the specimens were covered with Parafilm to avoid water loss. This stage of the

Table 1 Oxide analysis of the Portland cement and mineral admixtures used.

Oxide	OPC weight%	SF weight%	FA weight%
SiO_2	21.07	94.92	62.28
Al_2O_3	3.69	0.03	20.38
Fe_2O_3	4.50	0.03	4.09
CaO	61.93	0.56	4.68
TiO_2	0.97	< 0.02	0.94
P_2O_5	0.10	0.13	0.38
MgO	1.83	0.38	0.98
Na_2O	0.09	0.08	0.31
K_2O	0.30	0.86	0.99
SO_3	2.54	–	–
LOI	4.38	3.69	3.43

process was marked as day − 4. Subsequently, the Parafilm was removed and the specimens were oven dried at 105 °C until constant mass was achieved. This stage was marked as day − 1. The specimens were cooled and vacuum saturated (− 20 in-Hg) with NaCl solutions at concentrations of 0, 2.8, and 5.6 mol/L (day 0). Vacuum saturation was used to accelerate chloride ion ingress, and consequently chloride binding. The specimens were covered with Parafilm to prevent moisture loss.

After vacuum saturation of the specimens (day 0), the solutions left in the containers were brownish and included suspended particles that precipitated after 1 day. A Fourier transform infrared (FTIR) spectroscopy analysis of these particles indicated the presence of calcium carbonate produced by the reaction between the calcium hydroxide within the specimens and the carbon dioxide present in the solution.

2.2.2 Chloride Binding Isotherms

Chloride binding isotherms were determined for the four cement pastes in accordance with the technique proposed by Luping and Nilsson (1993). In this technique, the central regions of the specimens were cut into discs 5 mm thick, which were ground before being passed through a No. 8 sieve (2.5 mm) and retained in a No. 60 sieve (0.25 mm). Then, 15 g of ground paste was placed in 125 mL plastic bottles and vacuum saturated for 2 h. The bottles were filled with 60 mL of NaCl solutions at seven different concentrations (0.1, 0.3, 0.5, 0.7, 1.0, 2.0, and 3.0 mol/L), sealed and stored at 23 ± 1 °C. The changes in the chloride ion concentrations of NaCl solutions with initial concentrations of 3.0 mol/L were monitored as functions of time until the solution concentrations were constant, indicating that no further binding was occurring (Thomas et al. 2012). The amount of bound chlorides C_b, given in mg Cl/g of sample, was determined according to Eq. (1):

$$C_b = \frac{35.453V(C_i - C_e)}{W_{11}(1 - \xi_{11})} \quad (1)$$

where V is the volume of the external solution (mL), C_i is the initial chloride ion concentration of the external solution (mol/L), C_e is the concentration of free chloride ions in equilibrium with the external solution (mol/L), 35.453 is the molar mass of the chloride ion, W_{11} is the mass of the sample (g) and ξ_{11} is the evaporable water content (g). The last two parameters were determined at a relative humidity of 11%.

XRD measurements were performed in order to verify the formation of Friedel's salt. Friedel's salt is the main product of chemical chloride binding. The XRD spectra were obtained after the chloride binding isotherm experiments were complete. The cement pastes were dried at 105 °C for 24 h and then ground and passed through a No. 100 sieve (150 μm).

2.2.3 Ultrasonic Signal Acquisition

Through-transmission ultrasonic measurements with 500 kHz longitudinal wave transducers were performed on specimens saturated with the three NaCl solutions (0, 2.8, and 5.6 mol/L) 0, 1, 3, 7, 14, and 200 days after vacuum saturation. Measurements were also performed at − 4 and − 1 days. The specimen masses were measured before each ultrasonic measurement to detect significant moisture loss.

Sodium chloride solutions with concentrations of 0, 0.7, 1.4, 2.1, 2.8, 3.5, 4.2, 4.9, and 5.6 mol/L, contained in an extruded polystyrene vessel (65 mm in width × 65 mm in height × 100 mm in length) were subjected to ultrasonic pulses and their responses were recorded. Longitudinal wave contact transducers (500 kHz) were used in direct contact with the solutions. The UPVs (ACI Committee 228 2003) and signal energies (Lathi 1998) were calculated for all solutions. The energies were calculated as the sums of the squares of the amplitudes of the time-history responses. The resulting UPV and signal energy behavior detected in the solutions helped us to better understand the responses observed from the saturated cement paste specimens.

The excitation pulses used in all of the measurements were generated by an Olympus pulser/receiver model 5058PR with a voltage of 200 V, 20 Hz repetition rate, 500 Ω damping, and gains of 40 and 60 dB (applied to the OPC, 10SF samples; and to the 20FA, 40FA samples, respectively). Each condition had three replicate specimens. All of the pulse generation and the response signal acquisition parameters remained constant throughout the experiment.

3. Results and Discussion

3.1 Properties of the Hydrated Cement Pastes

The OPC, 10SF, and 20FA pastes had average moisture contents of 31% at 254 days, while the 40FA paste had an average moisture content of about 40%. The average variation in specimen moisture content (measured by mass) between the various testing days was about 0.033%, indicating negligible moisture loss during the ultrasonic measurements. Figure 1 presents the oven-dried bulk densities of the cement pastes, as well as their porosities. The higher porosity and lower density of the cement paste containing 40% FA results primarily from the relatively high cement

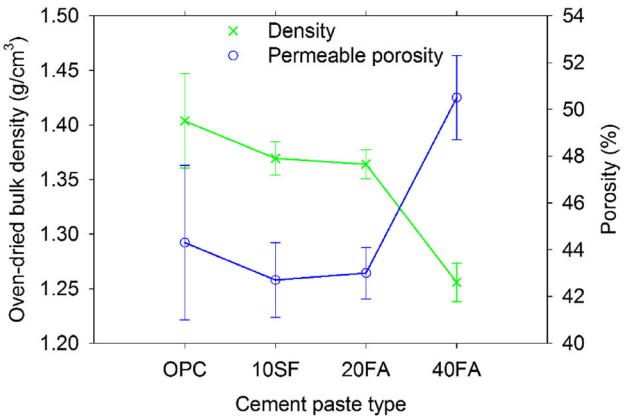

Fig. 1 Bulk densities and porosities of the cement pastes after oven drying (the error bars indicate ± one standard deviation).

replacement rate and the presence of unreacted fly ash, which acts as a low-density filler.

3.2 Chloride Binding

Variations in the external NaCl solution concentrations over time until equilibrium are shown in Fig. 2. Typically, when the ground cement pastes are immersed in a 3.0 mol/L NaCl solution, the external solution concentration stabilizes during the 3rd week. This is consistent with the stabilization times obtained by other researchers who used cement pastes with w/c values of 0.50 (Thomas et al. 2012; Zibara 2001) and 0.45 (Delagrave et al. 1997).

Titration of the seven NaCl solutions was performed in order to obtain the chloride binding isotherms presented in Fig. 3. The 40FA cement paste has the highest chloride binding capacity, followed in descending order by 10SF, 20FA, and OPC. These isotherms are in general agreement with behavior reported in the literature for these types of supplementary cementing materials (Delagrave et al. 1997; Thomas et al. 2012). The free chloride versus bound chloride data was plotted and fitted to Freundlich and Langmuir isotherms. The best fit is obtained with the Freundlich isotherm, which achieves a higher coefficient of determination ($R^2 = 0.99$) than the Langmuir isotherm ($R^2 = 0.96$). This is consistent with the results obtained by Zibara (2001), who found that data related to this level of NaCl concentration (higher than 0.01 mol/L) is best represented by the Freundlich isotherm (Eq. 2).

$$C_b = \alpha C_f^{\beta} \tag{2}$$

where α and β are binding constants and C_f is the concentration of free chloride ions (mol/L).

Friedel's salt is the result of chemical binding of chlorides to aluminates. Figure 4 presents XRD patterns that reveal the presence of Friedel's salt via peaks located at $2\theta = 11.3°$ with a net spacing of $d = 7.8$ Å. The peak intensities are related to the amount of Friedel's salt generated, which depends on the amount of tricalcium aluminate (C_3A) in the cement and alumina present in the supplementary cementing materials (Talero 2012). The 40FA paste produces the highest peak intensity, followed by 20FA, OPC, and 10SF. In addition, various levels of calcium hydroxide are observed in

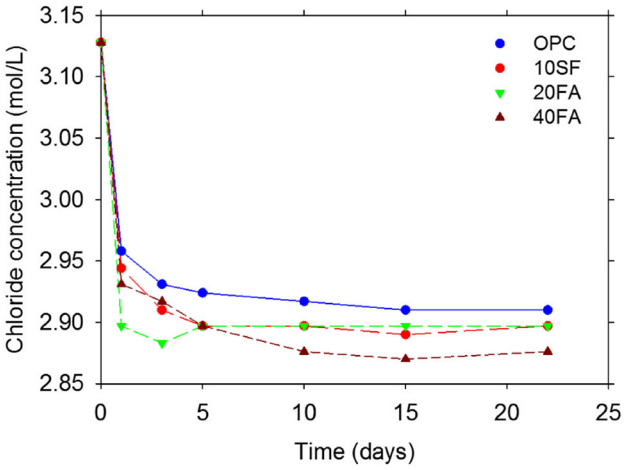

Fig. 2 Chloride concentrations of NaCl external solutions as a function of time.

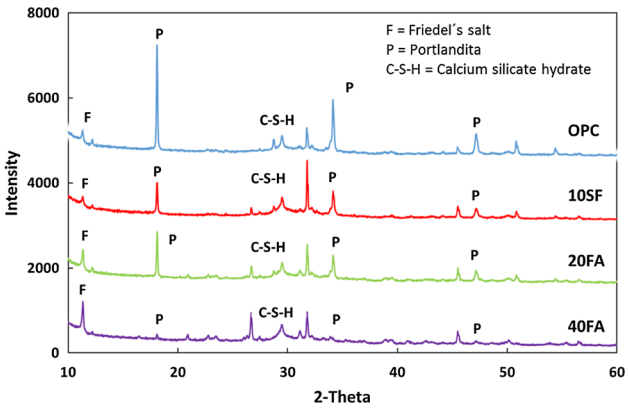

Fig. 4 XRD patterns of the cement pastes after equilibrium testing at 28 days.

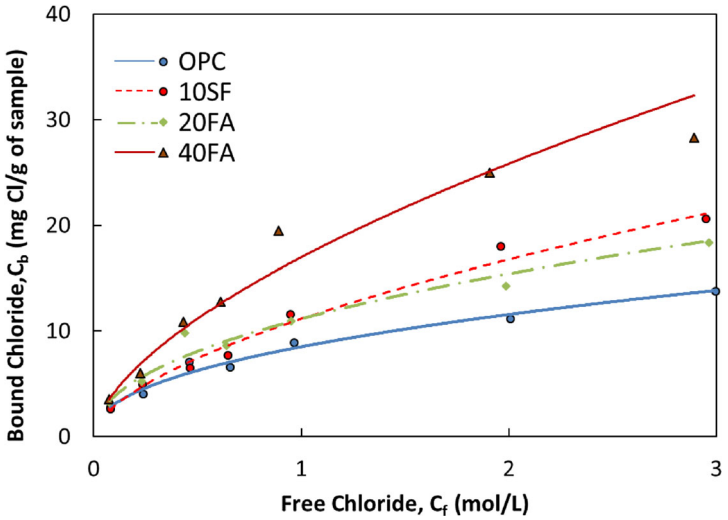

Fig. 3 Chloride binding isotherms of the cement pastes at 23 °C.

the cement pastes as a result of the pozzolanic reaction. This reaction reduces the amount of calcium hydroxide in pastes containing SF and FA.

Figure 5 shows the Friedel's salt XRD peak intensity and the alumina content, versus the amounts of bound chlorides in the pastes. Both graphs show that the bound chlorides increase with the alumina content in all cement pastes except for 10SF, which contains slightly less Al_2O_3 than OPC but provides the second highest binding capacity of the materials studied (Fig. 3). This confirms that SF contributes to binding by increasing chloride ion adsorption on the additional C–S–H produced by the pozzolanic reaction (Luping and Nilsson 1993). Generation of Friedel's salt is the dominant chloride binding process in the other cement pastes, as shown in Fig. 5. These results are consistent with those reported in the literature (Thomas et al. 2012; Zibara 2001), except that the literature indicates lower binding capacities among specimens that contain silica fume.

3.3 Ultrasonic Measurements

3.3.1 Signal Energies and UPVs in NaCl Solutions

Figure 6 presents ultrasonic characterizations of the NaCl solutions. Figure 6a and b show signal attenuation that arises from the fact that the solution viscosities increase with the NaCl concentration (Uedaira and Suzuki 1979). The frequency domain spectra of these signals show the "filtering" effect that higher concentration solutions apply to the ultrasonic response. Figure 6c shows the mean signal energies and mean UPVs of the tested solutions. The energy decreases as the NaCl concentration increases. This is because signal attenuation is enhanced when higher NaCl concentrations increase solution viscosities. In contrast, the UPV increases linearly when solution densities increase due to higher NaCl concentrations. These observations aid in interpretation of the results obtained with cement pastes. The porosities of the cement pastes are relatively high and thus their responses to ultrasonic pulses are significantly influenced by the characteristics of the solutions used for vacuum saturation.

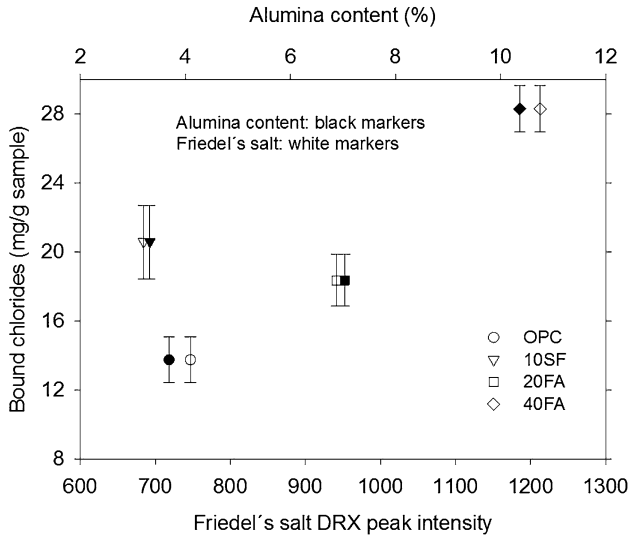

Fig. 5 Percentage of Al_2O_3 present in each paste and the Friedel's salt maximum intensity peak from XRD, versus the bound chlorides in cement pastes.

3.3.2 Effect of NaCl Solution Concentration on the Ultrasonic Responses of Cement Pastes

Figure 7 shows UPVs measured at various times before (day − 4) and after vacuum saturation (day 0) with deionized water and NaCl solutions at various concentrations. From the insets, it is evident that all of the pastes exhibit UPV decreases as a result of microcracking produced at day − 1 when the samples are oven-dried 105 °C (Bisschop and Wittel 2011; Wu et al. 2015). The effect of microcracking is so significant that the UPV does not recover to its initial value even after the cement pastes are vacuum saturated (day 0). After the specimens are vacuum saturated, the OPC, 10SF, and 20FA cement pastes exhibit nearly constant UPVs from days 1 through 200. In addition, slightly lower UPV values are observed in samples saturated with a 5.6 mol/L NaCl solution than in those saturated with 0 and 2.8 mol/L solutions. The 40FA cement paste samples saturated with - NaCl solutions present similar but more noticeable UPV behaviors. They exhibit relatively low UPV values from days 1 through 14, which increase from days 14 through 200. At days 0 and 1, only the 40FA cement paste exhibits UPV values that are consistent with the positive relationship between UPV and the NaCl concentration shown in Fig. 6c. After 1 day, this behavior changes only for the paste saturated with deionized water. It exhibits an exponential increase in UPV similar to that seen in typical cement hydration curves (Boumiz et al. 1996; Hewlett 2003) from 1 to 200 days.

Due to the levels of FA replacement and w/c ratios, the degree of cement hydration may be low (Lam et al. 2000), as may be the extent of the pozzolanic reaction (Sumranwanich and Tangtermsirikul 2004). After microcracking due to oven drying, unhydrated cement particles might become exposed and react with the saturating solution, generating new hydration products along these microcracks. Therefore, the UPV of the 40FA cement paste increases (Fig. 7d). It appears that rehydration is limited in samples that contain NaCl solutions and therefore is not high enough to seal the microcracks. This is in contrast to the behavior observed in the samples that are vacuum saturated with deionized water.

Now, let us use the energies of the ultrasonic signal response to identify the three NaCl solution concentrations within the cement pastes. The responses were recorded at − 4, − 1, 0, 1, 3, 7, 14, and 200 days. Figure 8 shows the signal energy evolution over time. Data for the OPC paste at day 0 saturated with the 5.6 mol/L NaCl solution was not recorded because the vacuum saturation period was longer than those of the rest of the specimens. Regardless of the type of cement paste, similar energy levels are observed from day − 4 (water saturated) to day − 1 (oven dried), which suggests similar paste microstructures after oven drying. However, the pastes exhibit distinct behaviors as time passes. There is an overall trend towards signal energy reduction as the NaCl concentration increases. Higher concentrations attenuate the signal (see Fig. 6c) by increasing

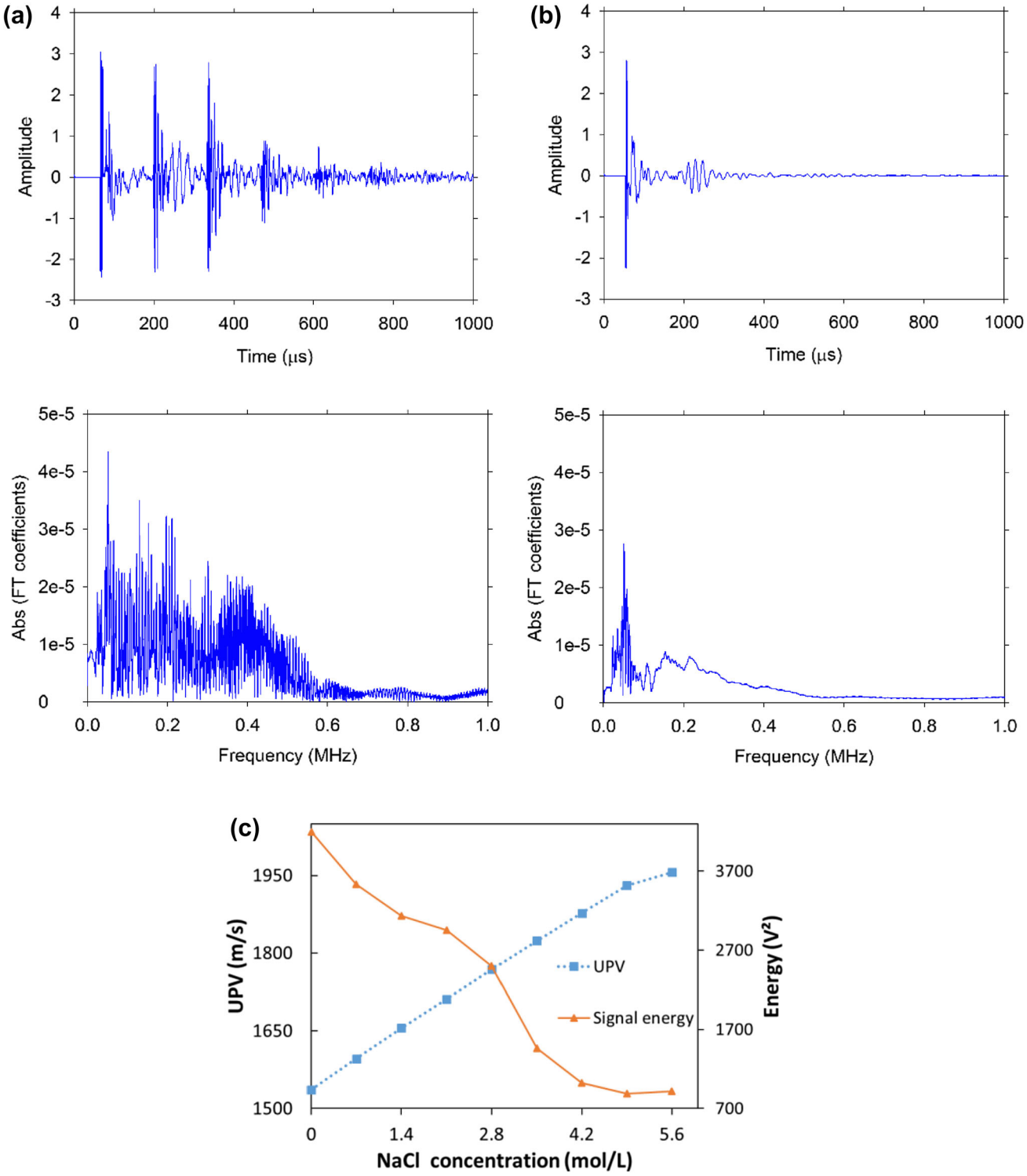

Fig. 6 Time and frequency domain ultrasonic responses of NaCl solutions at concentrations of **a** 0 mol/L, **b** 5.6 mol/L, and **c** Energies and UPVs of nine different NaCl solutions.

the pore fluid viscosity (Lin and Brown 1993) in the cement pastes. Upon comparing the distinct cement pastes, it is interesting to note the significant decreases in the energies of the 20FA and 40FA pastes compared to the OPC and 10SF pastes. This attenuation may be explained by chloride binding and scattering. Chloride binding produces a lower solution viscosity while generating Friedel's salt. Based on the low energies obtained with 20FA and 40FA, it is suggested that this reduction is produced by scattering caused by spherical particles of unreacted FA (Fig. 9) and Friedel's salt. The energy reductions observed in the 20FA and 40FA cement pastes vacuum saturated with deionized water are related to a similar process that occurs without generation of Friedel's salt. In the 40FA cement paste vacuum saturated with deionized water, the attenuation described also overcomes possible increases caused by new

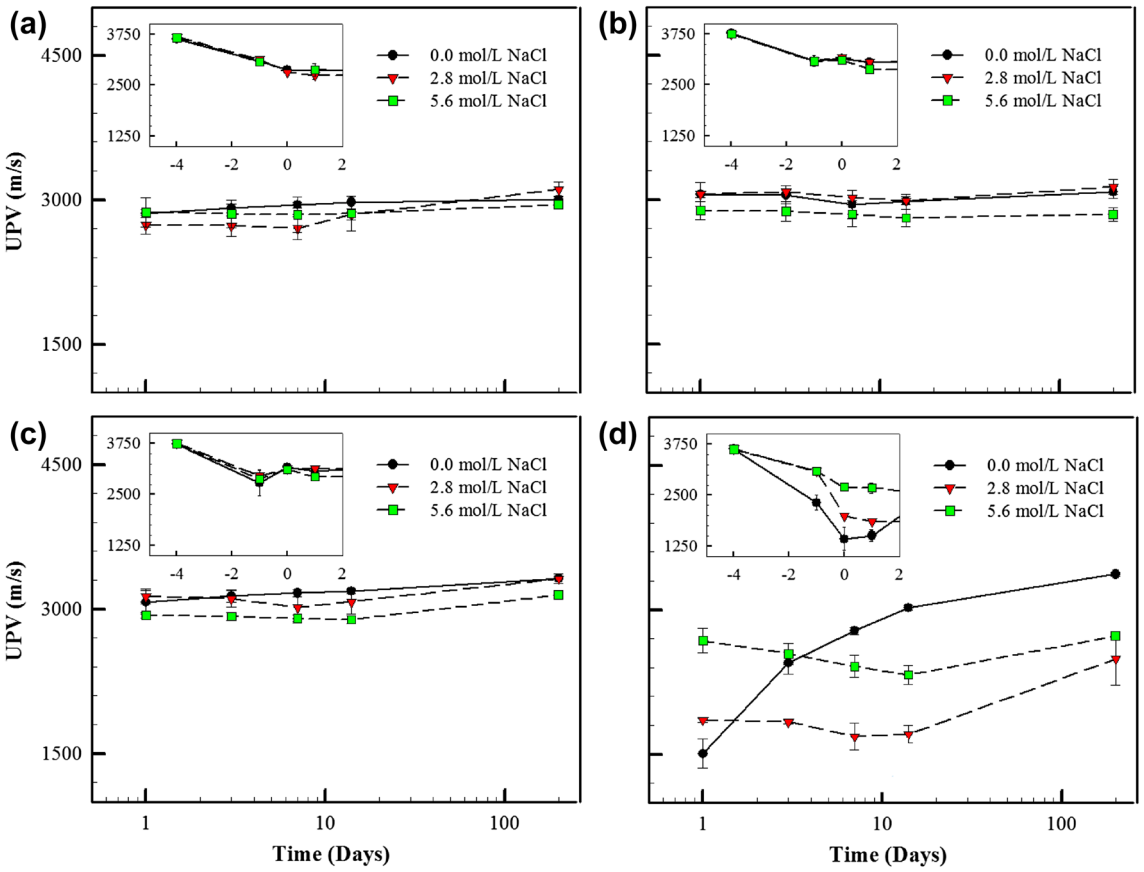

Fig. 7 UPVs in the following cement pastes: **a** OPC, **b** 10SF, **c** 20FA, and **d** 40FA.

generation of hydration products along the microcracks. The behavior of the 10SF paste differs from that described, probably because its chloride binding process (physical adsorption) is different from those of the other cement pastes (chemical binding).

Figure 10 shows the signal energies of all of the cement pastes at day 14 after vacuum saturation. The energies of the OPC and 10SF pastes are significantly higher than those of the 20FA and 40FA pastes at each NaCl concentration. The only exception is the OPC saturated with a 5.6 mol/L NaCl solution. As mentioned, the energy reductions in 20FA and 40FA are probably caused by chloride binding and scattering. Figure 2 suggests that most of the chloride ions should already be bound by day 14. This is indicated by the constant chloride concentrations of the external solutions. The pastes that have been treated with 0 and 2.8 mol/L NaCl solutions exhibit only moderate decreases in their signal energies. Distinctions between 2.8 and 5.6 mol/L are evident only for OPC. The change in the 10SF cement paste signal energy is less sensitive to the effects of NaCl concentration than the others. This is consistent with the fact that this cement paste undergoes a different chloride binding process and therefore impacts the energy of the ultrasonic signal response differently.

3.3.3 Ultrasonic Identification of Chloride Binding

The signal energy is presented in Fig. 11 as a function of testing time. This plot corresponds to pastes with a NaCl concentration of 2.8 mol/L (close to the maximum concentration of 3.0 mol/L used for the chloride binding isotherms). Before vacuum saturation (days − 4 and − 1) with the chloride solution, all of the pastes exhibit the same energy behavior. Thus, oven drying causes no significant differences between the microstructures of the cement pastes.

After vacuum saturation (> 0 days), the pastes containing 20FA and 40FA exhibit lower energies than the OPC and 10SF pastes. The larger volume of NaCl solution contained in the FA pastes (due to their higher porosities) might explain the more extensive decreases in the signal energies of these specimens. In addition, scattering caused by unreacted FA and the amorphous Friedel's salt generated might contribute to these energy decreases.

According to Fig. 2, the chloride binding processes stabilizes by day 14 in all of the pastes studied. As chemical binding of chlorides is closely related to the presence of aluminates, the relationship between the amounts of alumina and bound chlorides and the corresponding signal energies are presented in Fig. 12. Both relationships are similar, except in the case of bound chlorides where the cement paste containing SF behaves differently due to its different chloride binding mechanism. It is an outlier in the bound chloride-energy relationship.

Figure 13 shows the bound chlorides as functions of the amplitude weighted average frequency. The range of frequencies considered is limited by the sampling rate (25 MHz) and the duration of the signal (2.6214 ms). One

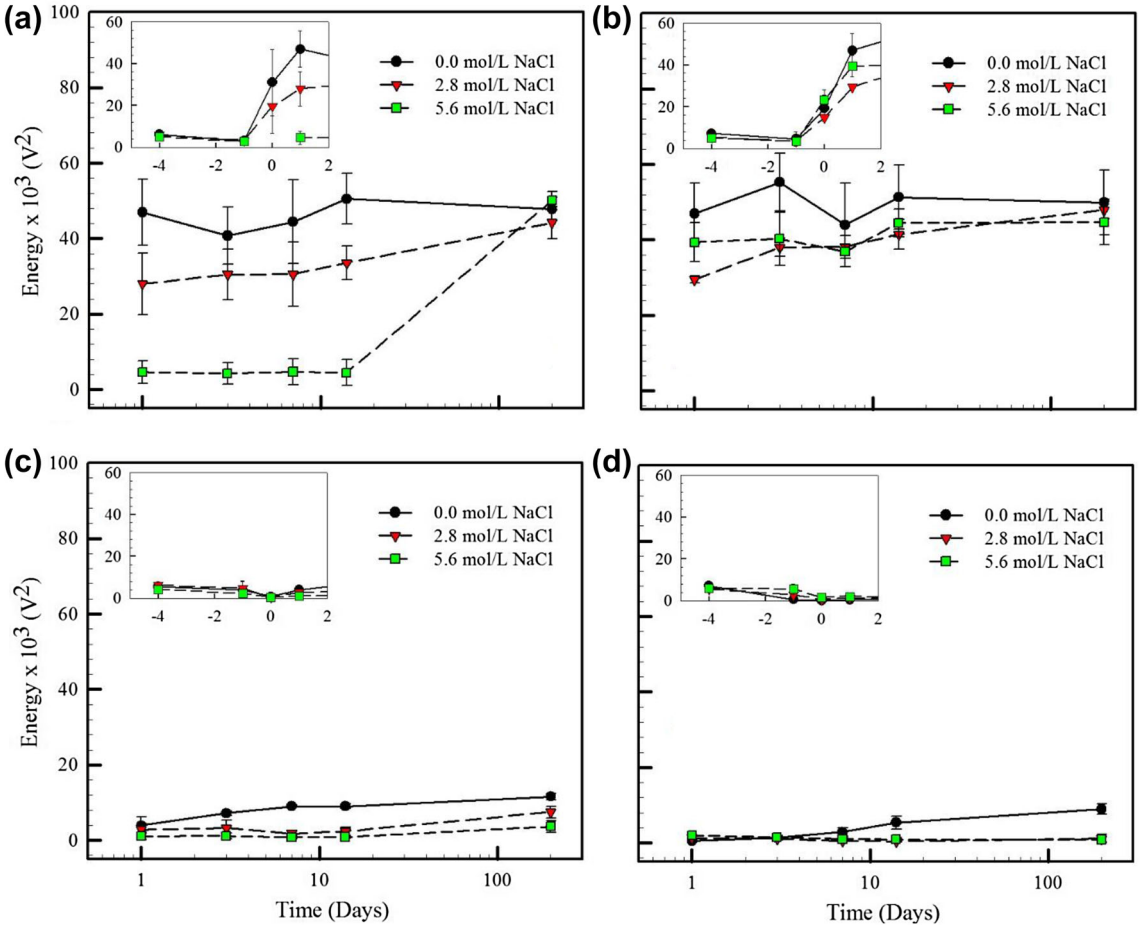

Fig. 8 Evolution of the energy over time of the specimen ultrasonic response (the error bars indicate ± one standard deviation), pastes **a** OPC, **b** 10SF, **c** 20FA, and **d** 40FA.

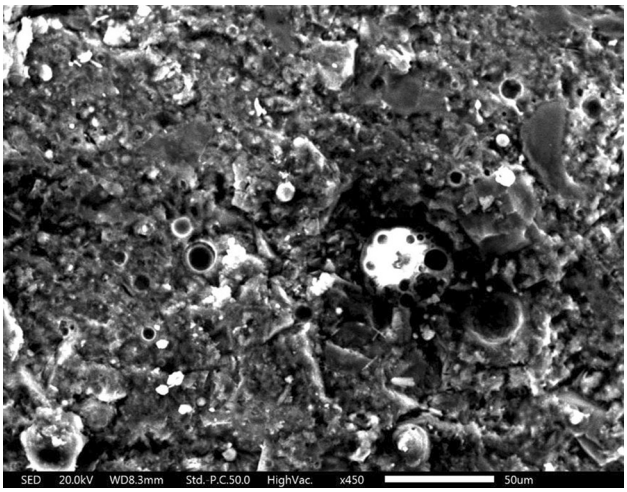

Fig. 9 Randomly distributed unreacted fly ash shown as hollow spherical particles in the 40FA cement paste.

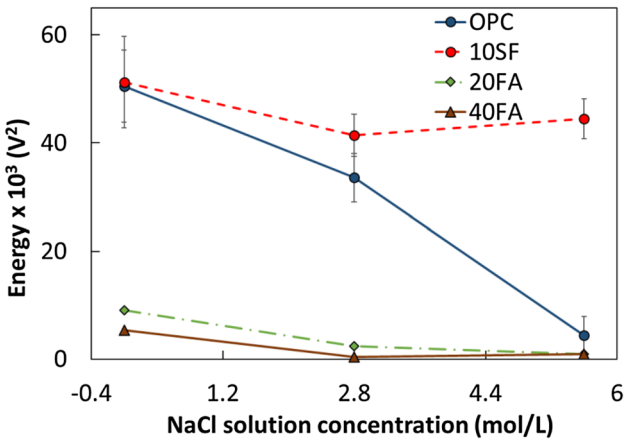

Fig. 10 Energy of the ultrasonic response at day 14 (the error bars indicate ± one standard deviation).

can note similarities between Figs. 5 and 12. In this case, the different chloride binding process in the 10SF paste is also evident. This demonstrates that the US signal response contains information related to both solid and pore fluid changes. Changes in the solid phase of the hydrated cement paste are produced via the generation of Friedel's salt. On the other hand, changes in the pore fluid occur due to reductions in chloride ion concentrations as chemical and physical binding occur.

Figure 14, a combination of Figs. 5 and 13, shows that the amplitude weighted average frequency from the ultrasonic measurements is related to the amounts of alumina and Friedel's salt present in the cement pastes. These results demonstrate that the ultrasonic responses of chloride-

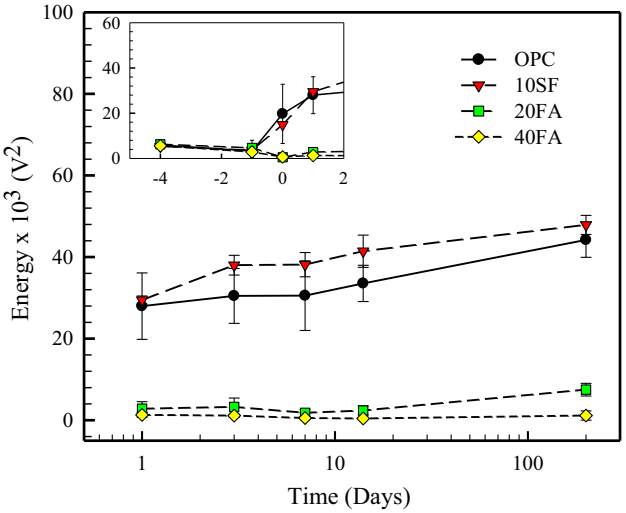

Fig. 11 Energy of the ultrasonic response of pastes vacuum saturated with a 2.8 mol/L NaCl solutions (the error bars indicate ± one standard deviation).

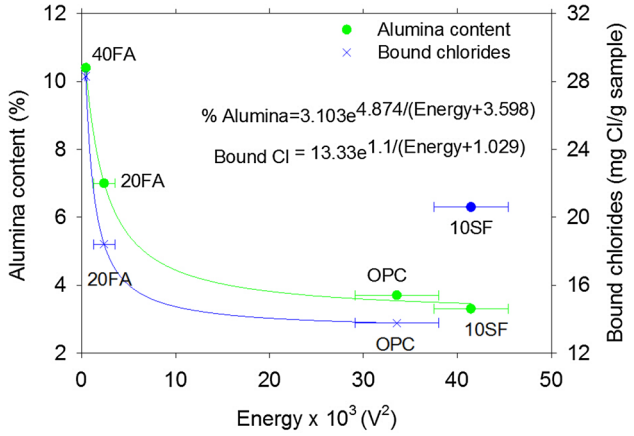

Fig. 12 Average energy of the ultrasonic response of pastes 14 days after vacuum saturation with a 2.8 mol/L NaCl solution, versus its corresponding alumina and bound chloride concentration.

containing cement pastes can be used to non-destructively study the chloride binding properties of cement-based materials.

4. Conclusions

This paper proposes the basis for an experimental monitoring technique based on US that can identify the presence of chloride solutions and their binding in four hydrated cement pastes. The ultrasonic responses of cement pastes after vacuum saturation with NaCl solutions of various concentrations were analyzed to identify relationships between the ultrasonic signal characteristics and binding capacities of the cement pastes. Based on the results obtained in the present research, the following conclusions are drawn:

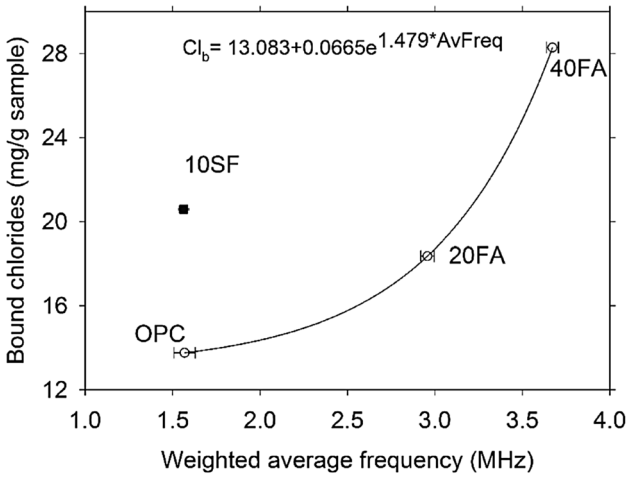

Fig. 13 Amplitude weighted average frequencies obtained from the Fourier spectra of ultrasonic response signals and the chloride binding capacities of the cement pastes (data correspond to pastes 14 days after vacuum saturation with a 2.8 mol/L NaCl solution).

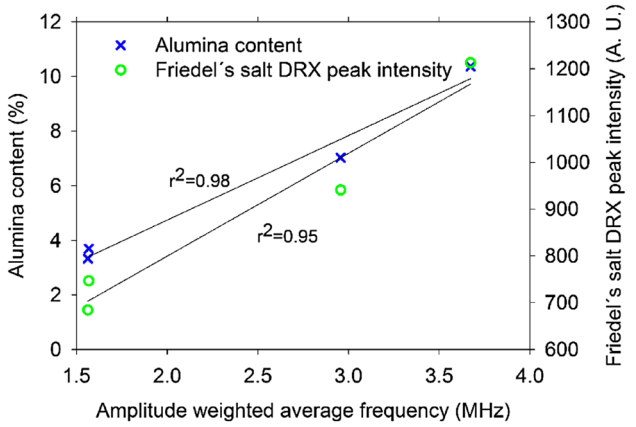

Fig. 14 Relationship between the amplitude weighted average frequency and the quantities of alumina and Friedel's salt present in the cement pastes.

(1) UPV measurements cannot detect either the type of fluid present in the cement pastes or the changes caused by chloride binding.
(2) The energy of the ultrasonic signal response allows identification of the NaCl solution concentration only for the OPC cement paste 14 days after vacuum saturation.
(3) There is an exponential decay relationship between the bound chlorides (governed by chemical reaction) and the signal energy, as well as between the alumina content and the signal energy.
(4) There is an exponential relationship between the amplitude weighted average frequency and the quantity of bound chloride (regulated by chemical reaction) in the cement paste.
(5) The amplitude weighted average frequency is directly proportional to the quantities of alumina and Friedel's salt generated by chemical chloride binding.

Although analysis of the results was challenging, especially with regard to the effect of microcracking on the energy results, promising non-destructive techniques for monitoring the durability of concrete structures may rely on the relationships found between signal energy (or amplitude weighted average frequency) and bound chloride (or alumina content). These relationships are valid only for those cement pastes which bind chlorides primarily via chemical reactions.

Acknowledgements

The authors acknowledge CONACyT and the Instituto Politecnico Nacional for financial support of the project (CONACyT CB Grant number 154552 and Grant number SIP 20131009, respectively). P. Cano acknowledges CONACyT of Mexico for financial support of the project with Grant Number 239727. Arturo Ramirez acknowledges CONACyT for his graduate studies scholarship. The authors acknowledge Dr. Mario F. Cosmes-López for his assistance during ultrasonic data acquisition.

Open Access

References

ACI Committee 228. (2003). In-Place Methods to Estimate Concrete Strength. *ACI Committee Reports*, (228, 1R), p. 41.

Aggelis, D. G., Shiotani, T., Momoki, S., & Hirama, A. (2009). Acoustic emission and ultrasound for damage characterization of concrete elements. *ACI Materials Journal, 106*(6), 509–514. https://doi.org/10.14359/51663333.

Al-Mattarneh, H. (2016). Determination of chloride content in concrete using near- and far-field microwave non-destructive methods. *Corrosion Science, 105*(Supplement C), 133–140. https://doi.org/10.1016/j.corsci.2016.01.010.

Andrade, C., d'Andrea, R., & Rebolledo, N. (2014). Chloride ion penetration in concrete: The reaction factor in the electrical resistivity model. *Cement and Concrete Composites, 47*(Supplement C), 41–46. https://doi.org/10.1016/j.cemconcomp.2013.09.022.

Angst, U., & Vennesland, Ø. (2009). Detecting critical chloride content in concrete using embedded ion selective electrodes—effect of liquid junction and membrane potentials. *Materials and Corrosion, 60*(8), 638–643. https://doi.org/10.1002/maco.200905280.

Ann, K. Y., & Song, H.-W. (2007). Chloride threshold level for corrosion of steel in concrete. *Corrosion Science, 49*(11), 4113–4133. https://doi.org/10.1016/j.corsci.2007.05.007.

ASTM C1202. (2012). Standard test method for electrical indication of concrete's ability to resist chloride ion penetration. *American Society for Testing and Materials*. https://doi.org/10.1520/C1202-12.2.

ASTM C305. (2011). Standard practice for mechanical mixing of hydraulic cement pastes and mortars of plastic consistency. *ASTM lnternational*. https://doi.org/10.1520/C0305-13.2.

Atkins, C. P., Scantlebury, J. D., Nedwell, P. J., & Blatch, S. P. (1996). Monitoring chloride concentrations in hardened cement pastes using ion selective electrodes. *Cement and Concrete Research, 26*(2), 319–324. https://doi.org/10.1016/0008-8846(95)00218-9.

Bisschop, J., & Wittel, F. K. (2011). Contraction gradient induced microcracking in hardened cement paste. *Cement & Concrete Composites, 33*(4), 466–473. https://doi.org/10.1016/j.cemconcomp.2011.02.004.

Boumiz, A., Vernet, C., & Cohen Tenoudji, F. (1996). Mechanical properties of cement pastes and mortars at early ages. *Advanced Cement Based Materials, 3*(3–4), 94–106. https://doi.org/10.1016/1065-7355(95)00072-0.

Byfors, K., Hansson, C. M., & Tritthart, J. (1986). Pore solution expression as a method to determine the influence of mineral additives on chloride binding. *Cement and Concrete Research, 16*(5), 760–770. https://doi.org/10.1016/0008-8846(86)90050-5.

Cano, F., Bremner, T. W., McGregor, R. P., & Balcom, B. J. (2002). Magnetic resonance imaging of ^{1}H, ^{23}Na, and ^{35}Cl penetration in Portland cement mortar. *Cement and Concrete Research, 32*(7), 1067–1070. https://doi.org/10.1016/S0008-8846(02)00747-0.

Chiniforush, A. A., Noushini, A., Akbarnezhad, A., & Valipour, H. (2017). Detecting the presence of chloride in hardened mortar using microwave non-destructive testing. In *High Tech Concrete: Where Technology and Engineering Meet - Proceedings of the 2017 fib Symposium* https://doi.org/10.1007/978-3-319-59471-2-11.

Delagrave, A., Marchand, J., Ollivier, J. P., Julien, S., & Hazrati, K. (1997). Chloride binding capacity of various hydrated cement paste systems. *Advanced Cement Based Materials, 6*(1), 28–35. https://doi.org/10.1016/S1065-7355(97)00007-2.

Dérobert, X., Lataste, J. F., Balayssac, J. P., & Laurens, S. (2017). Evaluation of chloride contamination in concrete using electromagnetic non-destructive testing methods. *NDT and E International, 89,* 19–29. https://doi.org/10.1016/j.ndteint.2017.03.006.

Falciai, R., Mignani, A. G., & Vannini, A. (2001). Long period gratings as solution concentration sensors. *Sensors and Actuators B: Chemical, 74*(1), 74–77. https://doi.org/10.1016/S0925-4005(00)00714-0.

Gao, P., Wei, J., Zhang, T., Hu, J., & Yu, Q. (2017). Modification of chloride diffusion coefficient of concrete based on the electrical conductivity of pore solution. *Construction*

and Building Materials, 145, 361–366. https://doi.org/10.1016/j.conbuildmat.2017.03.220.

Glass, G. K., & Buenfeld, N. R. (1997). The presentation of the chloride threshold level for corrosion of steel in concrete. *Corrosion Science, 39*(5), 1001–1013. https://doi.org/10.1016/S0010-938X(97)00009-7.

Gong, P., Patton, M. E., Liu, C., Oppenheim, I. J., Greve, D. W., Harley, J. B., & Junker, W. R. (2014). Ultrasonic detection of the alkali-silica reaction damage in concrete. In *IEEE International Ultrasonics Symposium, IUS* (pp. 361–364). https://doi.org/10.1109/ultsym.2014.0089.

Grantham, M. (2003). Diagnosis, inspection, testing and repair of reinforced concrete structures. *Advanced Concrete Technology.* https://doi.org/10.1016/b978-075065686-3/50269-x.

Herzfeld, K. F., & Litovitz, T. A. (2013). *Absorption and dispersion of ultrasonic waves*. New York: Academic Press.

Hewlett, P. (2003). *Lea's chemistry of cement and concrete*. (P. Hewlett, Ed.) (4th ed.). London: Butterworth-Heinemann.

Hirao, H., Yamada, K., Takahashi, H., & Zibara, H. (2005). Chloride binding of cement estimated by binding isotherms of hydrates. *Journal of Advanced Concrete Technology, 3*(1), 77–84. https://doi.org/10.3151/jact.3.77.

Hornbostel, K., Larsen, C. K., & Geiker, M. R. (2013). Relationship between concrete resistivity and corrosion rate—A literature review. *Cement & Concrete Composites*. https://doi.org/10.1016/j.cemconcomp.2013.03.019.

Hugenschmidt, J., & Loser, R. (2007). Detection of chlorides and moisture in concrete structures with Ground Penetrating Radar. *EMPA Activities, 2007,* 37. https://doi.org/10.1617/s11527-007-9282-5.

Jin, M., Jiang, L., & Zhu, Q. (2017). Monitoring chloride ion penetration in concrete with different mineral admixtures based on embedded chloride ion selective electrodes. *Construction and Building Materials, 143,* 1–15. https://doi.org/10.1016/j.conbuildmat.2017.03.131.

Ju, T., Achenbach, J. D., Jacobs, L. J., Guimaraes, M., & Qu, J. (2017). Ultrasonic nondestructive evaluation of alkali–silica reaction damage in concrete prism samples. *Materials and Structures, 50*(1), 60. https://doi.org/10.1617/s11527-016-0869-6.

Jung, Y. C., Kundu, T., & Ehsani, M. R. (2002). A new non-destructive inspection technique for reinforced concrete beams. *ACI Materials Journal, 99*(3), 292–299.

Kalogeropoulos, A., Van Der Kruk, J., Hugenschmidt, J., Bikowski, J., & Brühwiler, E. (2013). Full-waveform GPR inversion to assess chloride gradients in concrete. *NDT and E International, 57,* 74–84. https://doi.org/10.1016/j.ndteint.2013.03.003.

Lafhaj, Z., Goueygou, M., Djerbi, A., & Kaczmarek, M. (2006). Correlation between porosity, permeability and ultrasonic parameters of mortar with variable water/cement ratio and water content. *Cement and Concrete Research, 36*(4), 625–633. https://doi.org/10.1016/j.cemconres.2005.11.009.

Lam, C. C. C., Mandamparambil, R., Sun, T., Grattan, K. T. V., Nanukuttan, S. V., Taylor, S. E., et al. (2009). Optical fiber refractive index sensor for chloride ion monitoring. *IEEE Sensors Journal, 9*(5), 525–532. https://doi.org/10.1109/JSEN.2009.2016597.

Lam, L., Wong, Y. L., & Poon, C. S. (2000). Degree of hydration and gel/space ratio of high-volume fly ash/cement systems. *Cement and Concrete Research, 30*(5), 747–756. https://doi.org/10.1016/S0008-8846(00)00213-1.

Lathi, B. P. (1998). *Signal Processing and Linear Systems*. (B. C. Press, Ed.) *Berkeley Cambridge Press*. New York: Oxford University Press.

Lee, H. K., Lee, K. M., Kim, Y. H., Yim, H., & Bae, D. B. (2004). Ultrasonic in situ monitoring of setting process of high-performance concrete. *Cement and Concrete Research, 34*(4), 631–640. https://doi.org/10.1016/j.cemconres.2003.10.012.

Lin, J., & Brown, C. W. (1993). Simultaneous determination of physical and chemical properties of sodium chloride solutions by near infrared spectroscopy. *Near Infrared Spectroscopy, 1*(1), 109. https://doi.org/10.1255/jnirs.14.

Luping, T., & Nilsson, L. O. (1993). Chloride binding capacity and binding isotherms of OPC pastes and mortars. *Cement and Concrete Research, 23*(2), 247–253. https://doi.org/10.1016/0008-8846(93)90089-R.

Marinescu, M., & Brouwers, J. (2012). Chloride binding related to hydration products part I: Ordinary Portland cement. *Cement and Concrete Research, 3,* 125–131. https://doi.org/10.1007/978-94-007-2703-8_13.

Neville, A. (1995). Chloride attack of reinforced concrete: an overview. *Materials and Structures, 28*(2), 63–70. https://doi.org/10.1007/BF02473172.

NT BUILD-443. (1995). Concrete Hardened: Accelerated chloride penetration. *Nordtest method Finland*, pp. 1–5.

NT BUILD-492. (1999). Concrete, mortar and cement-based repair materials: chloride migration coefficient from non-steady-state migration experiments. *Nordtest Method Finland, 492,* 1–8.

Ohdaira, E., & Masuzawa, N. (2000). Water content and its effect on ultrasound propagation in concrete—the possibility of NDE. *Ultrasonics, 38*(1), 546–552. https://doi.org/10.1016/S0041-624X(99)00158-4.

Paul, G., Boccaleri, E., Buzzi, L., Canonico, F., & Gastaldi, D. (2015). Friedel's salt formation in sulfoaluminate cements: A combined XRD and ^{27}Al MAS NMR study. *Cement and Concrete Research, 67,* 93–102. https://doi.org/10.1016/j.cemconres.2014.08.004.

Polder, R. B., & Peelen, W. H. A. (2002). Characterisation of chloride transport and reinforcement corrosion in concrete under cyclic wetting and drying by electrical resistivity. *Cement & Concrete Composites, 24*(5), 427–435. https://doi.org/10.1016/S0958-9465(01)00074-9.

Povey, M. (1997). *Ultrasonic Techniques for Fluids Characterization*. New York: Academic Press.

Punurai, W., Jarzynski, J., Qu, J., Kim, J. Y., Jacobs, L. J., & Kurtis, K. E. (2007). Characterization of multi-scale porosity in cement paste by advanced ultrasonic techniques. *Cement and Concrete Research, 37*(1), 38–46. https://doi.org/10.1016/j.cemconres.2006.09.016.

Saremi, M., Mahallati, E., Sieber, J., Broton, D., Fales, C., Leigh, S., et al. (2002). A study on chloride-induced depassivation of mild steel in simulated concrete pore solution. *Cement*

and Concrete Research, 32(12), 1915–1921. https://doi.org/10.1016/S0008-8846(02)00895-5.

Senin, S. F., & Hamid, R. (2016). Ground penetrating radar wave attenuation models for estimation of moisture and chloride content in concrete slab. *Construction and Building Materials, 106,* 659–669. https://doi.org/10.1016/j.conbuildmat.2015.12.156.

Sumranwanich, T., & Tangtermsirikul, S. (2004). A model for predicting time-dependent chloride binding capacity of cement-fly ash cementitious system. *Materials and Structures, 37*(6), 387–396. https://doi.org/10.1007/BF02479635.

Suryavanshi, A. K., Scantlebury, J. D., & Lyon, S. B. (1996). Mechanism of Friedel's salt formation in cements rich in tri-calcium aluminate. *Cement and Concrete Research, 26*(5), 717–727. https://doi.org/10.1016/S0008-8846(96)85009-5.

Talero, R. (2012). Synergic effect of Friedel's salt from pozzolan and from OPC co-precipitating in a chloride solution. *Construction and Building Materials, 33,* 164–180. https://doi.org/10.1016/j.conbuildmat.2011.12.040.

Thomas, M. D., Hooton, R. D., Scott, A., & Zibara, H. (2012). The effect of supplementary cementitious materials on chloride binding in hardened cement paste. *Cement and Concrete Research, 42*(1), 1–7. https://doi.org/10.1016/j.cemconres.2011.01.001.

Torres-Luque, M., Bastidas-Arteaga, E., Schoefs, F., Sánchez-Silva, M., & Osma, J. F. (2014). Non-destructive methods for measuring chloride ingress into concrete: State-of-the-art and future challenges. *Construction and Building Materials*. https://doi.org/10.1016/j.conbuildmat.2014.06.009.

Trtnik, G., Valič, M. I., & Turk, G. (2013). Measurement of setting process of cement pastes using non-destructive ultrasonic shear wave reflection technique. *NDT and E International, 56,* 65–75. https://doi.org/10.1016/j.ndteint.2013.02.004.

Uedaira, H., & Suzuki, Y. (1979). Ultrasonic velocity and compressibility in aqueous solutions of alkali metal chlorides. *Bulletin of the Chemical Society of Japan, 52*(10), 2787–2790. https://doi.org/10.1246/bcsj.52.2787.

Wu, Z., Wong, H. S., & Buenfeld, N. R. (2015). Influence of drying-induced microcracking and related size effects on mass transport properties of concrete. *Cement and Concrete Research, 68,* 35–48. https://doi.org/10.1016/j.cemconres.2014.10.018.

Zibara, H. (2001). *Binding of external chlorides by cement pastes*. *PhD Thesis*. University of Toronto, PhD Thesis. Retrieved from https://tspace.library.utoronto.ca/bitstream/1807/15366/1/NQ63607.pdf.